Acta Biomaterialia 92 (2019) 196–204

Contents lists available at ScienceDirect

Acta Biomaterialia

journal homepage: www.elsevier.com/locate/actabiomat

Full length article

Low-toxicity transferrin-guided polymersomal doxorubicin for potent chemotherapy of orthotopic hepatocellular carcinoma *in vivo*

Yaohua Wei [a,b], Xiaolei Gu [a], Liang Cheng [a,c,*], Fenghua Meng [a,*], Gert Storm [b], Zhiyuan Zhong [a,*]

[a] Biomedical Polymers Laboratory, College of Chemistry, Chemical Engineering and Materials Science, and State Key Laboratory of Radiation Medicine and Protection, Soochow University, Suzhou 215123, PR China
[b] Department of Biomaterials Science and Technology, MIRA Institute for Biological Technology and Technical Medicine, University of Twente, PO Box 217, 7500AE Enschede, The Netherlands
[c] Department of Pharmaceutics, College of Pharmaceutical Sciences, Soochow University, Suzhou 215123, PR China

ARTICLE INFO

Article history:
Received 23 January 2019
Received in revised form 6 May 2019
Accepted 13 May 2019
Available online 15 May 2019

Keywords:
Transferrin
Polymersomes
Reduction-sensitive
Targeted delivery
Liver cancer

ABSTRACT

Hepatocellular carcinoma (HCC) remains one of the most lethal malignancies. The current chemotherapy with typically low tumor uptake and high toxicity reveals a poor anti-HCC efficacy. Here, we report transferrin-guided polycarbonate-based polymersomal doxorubicin (Tf-Ps-Dox) as a low-toxic and potent nanotherapeutic agent for effective treatment of liver tumor using a transferrin receptor (TfR)-positive human liver tumor SMMC-7721 model. Tf-Ps-Dox was facilely fabricated with small size of ca. 75 nm and varying Tf densities from 2.2% to 7.0%, by postmodification of maleimide-functionalized Ps-Dox (Dox loading content of 10.6 wt%) with thiolated transferrin. MTT assays showed that Tf-Ps-Dox had an optimal Tf surface density of 3.9%. The cellular uptake, intracellular Dox level, and anticancer efficacy of Tf-Ps-Dox to SMMC-7721 cells were inhibited by supplementing free transferrin, which supports that Tf-Ps-Dox is endocytosed through TfR. Interestingly, Tf-Ps-Dox exhibited a high accumulation of 8.5% ID/g (percent injected dose per gram of tissue) in subcutaneous SMMC-7721 tumors, which was 2- and 3-fold higher than that of nontargeted Ps-Dox and clinically used liposomal Dox formulation (Lipo-Dox), respectively. The median survival times of mice bearing orthotopic SMMC-7721 tumors increased from 82, 88 to 96 days when treated with Tf-Ps-Dox at Dox doses from 8, 12 to 16 mg/kg, which was significantly longer than that of Ps-Dox at 8 mg/kg (58 days) and Lipo-Dox at 4 mg/kg (48 days) or PBS (36 days). Notably, unlike Lipo-Dox, no body weight loss and damage to major organs could be discerned for all Tf-Ps-Dox groups, indicating that Tf-Ps-Dox caused low systemic toxicity. This transferrin-dressed polymersomal doxorubicin provides a potent and low-toxic treatment modality for human hepatocellular carcinoma.

Statement of Significance

Hepatocellular carcinoma (HCC) is one of the leading causes of cancer-related death worldwide. Vast work has focused on developing HCC-targeted nanotherapeutics. However, none of the nanotherapeutics has advanced to clinics, partly because the ligands used have not been validated in patients. Transferrin (Tf) is a natural ligand for transferrin receptor (TfR) that is overexpressed on cancerous cells, and it is currently under clinical trials (MBP-426 and CALAA-01) for the treatment of solid tumors. We designed Tf-functionalized polymersomal doxorubicin (Tf-Ps-Dox) for targeted therapy of orthotopic SMMC-7721 tumor in nude mice. Tf-Ps-Dox showed potent anti-HCC efficacy and significantly improved survival time with low toxicity as compared with nontargeted Ps-Dox and clinical liposomal Dox (Lipo-Dox). Hence, Tf-Ps-Dox is very appealing for targeted treatment of HCC.

1. Introduction

Hepatocellular carcinoma (HCC) is the leading cause of cancer-related death worldwide [1]. The major clinical treatments for HCC include conventional surgery, liver transplantation, trans-arterial chemoembolization, and small kinase inhibitors [2–4]. Traditional

* Corresponding authors at: Biomedical Polymers Laboratory, College of Chemistry, Chemical Engineering and Materials Science, and State Key Laboratory of Radiation Medicine and Protection, Soochow University, Suzhou 215123, PR China (Z. Zhong, F. Meng, L. Cheng).
E-mail addresses: chengliang1983@suda.edu.cn (L. Cheng), fhmeng@suda.edu.cn (F. Meng), zyzhong@suda.edu.cn (Z. Zhong).

https://doi.org/10.1016/j.actbio.2019.05.034
1742-7061/

chemotherapeutic agents are not effective and further associated with severe side effects as a result of poor HCC-specificity [5]. The development of HCC-targeted nanotherapeutics has been regarded as a valuable solution to HCC chemotherapy [6–18]. Antibodies and peptides were routinely used as targeting ligands for HCC treatment. For instance, CD44 antibody-targeted liposomal nanoparticles were used for molecular imaging and therapy of HCC [19]. The SP94 peptide-decorated Pt nanocluster assembly was used to overcome cisplatin resistance for anti-HCC therapy [20]. However, none of these novel HCC-targeted nanoformulations has moved forward to clinical trials, partly because these targeting ligands have not been validated in patients. Furthermore, although galactosamine-PHPMA-GFLG-Dox (PK2) has been translated to human clinical trials, the expression of the asialoglycoprotein receptor (ASGP-R) on mammalian hepatocytes leads to low HCC-specificity [21].

Transferrin receptor (TfR) is overexpressed on many cancerous cells including SMMC-7721 [22], MDA-MB 231 [23], U87-MG [24], and A549 cells [25] owing to abnormal iron metabolism [26]. Transferrin (Tf), an endogenous protein that serves to translocate iron into TfR-overexpressed cells, is known as a natural ligand for TfR [27]. Tf has been employed as a specific carrier for different drugs [28,29] or targeting ligand for various nanoformulations [30–37]. Notably, several targeted nanomedicines homing to TfR are currently under clinical trials [38]. For instance, Tf-modified lipid formulation of oxaliplatin, MBP-426, from Mebiopharm has entered Phase II clinical trials for metastatic gastric, gastro-esophageal junction, and esophageal adenocarcinoma [39]. Tf-targeted RRM2 siRNA formulation, CALAA-01, from Calando Pharmaceuticals has been tested for the treatment of patients with solid tumor [40,41].

Here, we report on Tf-functionalized, polycarbonate-based polymersomal Dox (Tf-Ps-Dox) for targeted therapy of orthotopic SMMC-7721 HCC in nude mice (Scheme 1). The polymersomes were prepared by co-self-assembly of biodegradable copolymer poly(ethylene glycol)-*b*-poly(trimethylene carbonate-*co*-dithiolane trimethylene carbonate) (mPEG-P(TMC-DTC), M_n = 5.0–14.8–1.9 kg/mol) and maleimide-functionalized copolymer (Mal-PEG-P(TMC-DTC), M_n = 7.5–15.5–2.2 kg/mol). We reported that the Ps-Dox has outstanding stability, high tolerability, and reduction-triggered drug release behavior [42]. The high stability of Ps-Dox allows facile surface conjugation with targeting ligands by the postmodification method. In this study, the post-modification of Ps-Dox with Tf, the influence of Tf density on targeting ability of Ps-Dox, and the therapeutic efficacy of Tf-Ps-Dox toward TfR-overexpressing hepatocellular carcinoma were investigated.

2. Experimental section

2.1. Formation of maleimide-functionalized polymersomal doxorubicin (Mal-Ps-Dox)

Mal-Ps-Dox was obtained first by self-assembly of poly(ethylene glycol)-*b*-poly(trimethylene carbonate-*co*-dithiolane trimethylene carbonate) (mPEG-P(TMC-DTC)) and maleimide-functionalized copolymer Mal-PEG-P(TMC-DTC) and then by active loading of Dox·HCl using a pH-gradient method [42]. In a typical example, 100 μL of DMF solution of the mPEG-P(TMC-DTC) and Mal-PEG-P(TMC-DTC) mixture (molar ratio = 95/5, polymer concentration = 40 mg/mL) was added dropwise into 900 μL of citric acid buffer (10 mM, pH 4.0). After standing still for 1 h, the pH was adjusted to 7.8 using saturated Na_2HPO_4 solution. Then 160 μL of Dox·HCl aqueous solution (5 mg/mL, theoretical drug loading content (DLC) = 16.7 wt%) was added and incubated at 37 °C for 12 h under mild stirring before 6 h dialysis (MWCO 7000 Da). During the workup procedure, the thus-obtained Mal-Ps-Dox was self-crosslinked. The Dox loading level was quantified using UV–Vis spectroscopy (UH5300, Hitachi, Japan) at an excita-

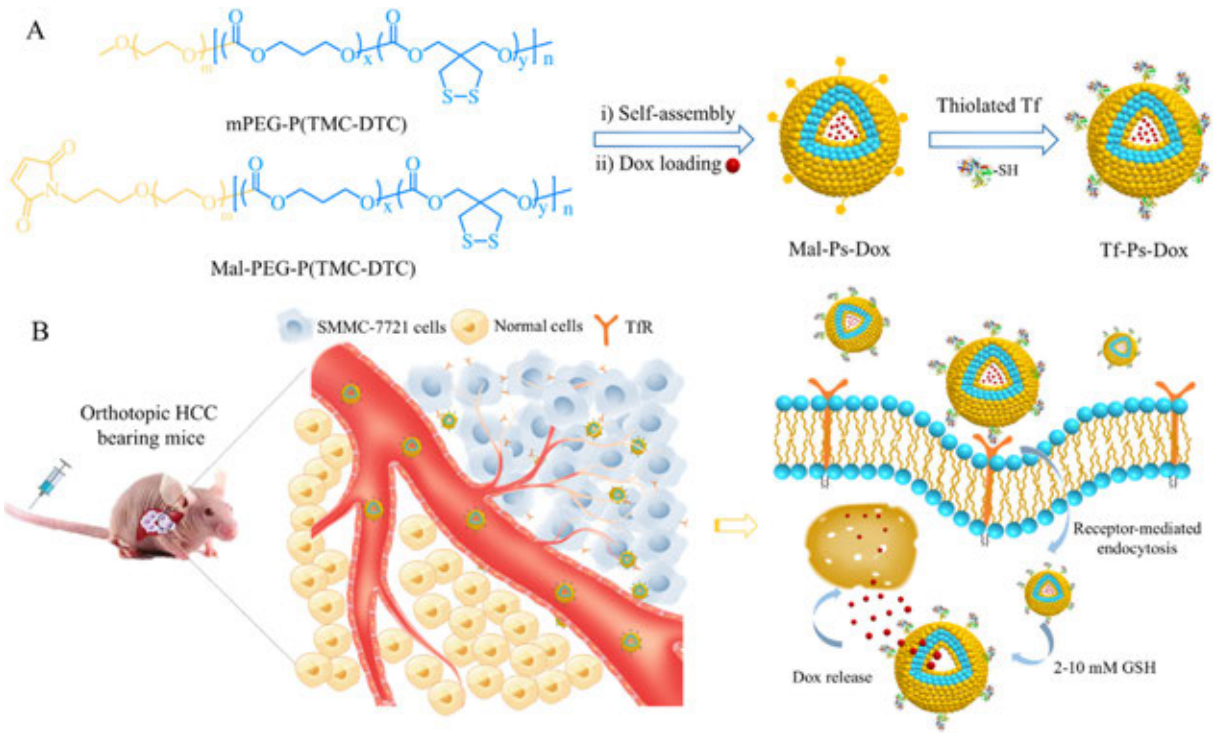

Scheme 1. Schematic illustration of preparation of transferrin-guided, reduction-responsive and reversibly cross-linked polymersomal doxorubicin (Tf-Ps-Dox) (A), and the targeted therapy of orthotopic hepatocellular carcinoma of Tf-Ps-Dox *in vivo* (B).

tion wavelength of 480 nm. Drug loading efficiency (DLE) and DLC were determined using the following formula:

DLE (%) = (weight of loaded Dox/weight of Dox in feed) × 100
DLC (wt.%) = (weight of loaded Dox/total weight of polymer and Dox) × 100.

2.2. Preparation of Tf-Ps-Dox

Tf-Ps-Dox was prepared by postmodification of Mal-Ps-Dox with thiolated transferrin (Tf-SH). Tf was thiolated using 2-iminothiolane hydrochloride (Traut's Reagent, TRC) under nitrogen atmosphere. In brief, 22 μL of TRC solution (10 mg/mL) in 10 mM HEPES (pH 8.0) containing 2 mM EDTA was added into 1 mL of Tf solution (10 mg/mL) in the same media, to result in a final TRC/Tf molar ratio of 10/1. The reaction proceeded at 37 °C for 1 h. The excess TRC was removed by repeated centrifugal ultrafiltration (Millipore, MWCO 10,000 Da). The extent of thiolation as determined by Ellman's assay [43] was four thiol groups per transferrin. Then, Tf-SH was added into 1 mL freshly obtained Mal-Ps-Dox at a molar ratio of Tf-SH/Maleimide of 2/1. After reaction at 37 °C for 8 h, free Tf was removed by centrifugal ultrafiltration (Millipore, MWCO 100,000 Da) twice at 3000*g* for 10 min. Tf was quantified using BCA assays based on a standard curve of protein solutions of known concentrations, and the conjugation efficiency (the ratio of Tf and polymer) was then calculated.

2.3. MTT assays

Human hepatocellular carcinoma SMMC-7721 cells were seeded in a 96-well plate (5×10^3 cells/well) for 24 h to reach 70% confluence. Tf-Ps-Dox (5 μg Dox/mL; 20 μL) with Tf molar contents of 2.2%, 3.9%, 6.0%, and7.0% was added to the cells, and the plate was incubated for 2 h. The media were substituted with fresh media, and the cells were cultured further for 70 h. MTT in PBS (10 μL, 5 mg/mL) was then added to the cells for 4 h before adding 150 μL of DMSO to dissolve MTT-formazan. The absorbance at 492 nm was measured using a microplate reader. The cells were co-incubated with 20-fold excess transferrin (1 mg/mL) and Tf-Ps-Dox for 2 h to verify the receptor-mediated endocytosis mechanism. Tf-Ps-Dox was used as controls.

2.4. Flow cytometry and confocal laser scanning microscopy (CLSM) studies

Flow cytometry was employed to investigate the cellular uptake of Tf-Ps-Dox. SMMC-7721 cells seeded in a 6-well plate (5×10^5 cells/well) were incubated with Tf-Ps-Dox (Tf molar contents of 2.2%, 3.9%, 6.0%, and 7.0%), Ps-Dox (10 μg DOX/mL), and PBS at 37 °C for 2 h. To prove receptor-mediated endocytosis, 20-fold excess transferrin (1 mg/mL) was co-incubated with Tf-Ps-Dox. After washing twice with PBS, the cells were detached, centrifuged, dispersed in 500 μL of PBS, and immediately measured using a BD FACSCalibur Flow Cytometer at FL2-channel (ex. 488 nm, em. 560 nm). For each sample, 10,000 events were collected.

For CLSM measurements, Tf-Ps-Dox was added (100 μL, 10 μg DOX/mL) to SMMC-7721 cells seeded on coverslips in a 24-well plate. After 2 h, the cells were fixed with 4% paraformaldehyde solution and the nuclei were stained with 4′,6′-diamidino-2-pheny lindole (DAPI) for 10 min before CLSM observation. PBS washing (×3) was applied between two steps. The inhibition experiment was conducted by adding 20-fold excess transferrin (1 mg/mL) in the culture medium. The same settings of CLSM were used for both groups. A 405 nm diode laser was selected for DAPI channel, and the laser power was adjusted to 3%. An argon laser was selected for doxorubicin acquisition, and the power was adjusted to 13%. The scan speed was 200 Hz, with a resolution of 1024 × 1024. The PMT intensity of DAPI was 20% and 60% for doxorubicin smart gain (HyD), respectively.

2.5. Animal models

The subcutaneous and orthotopic liver tumor models in female BALB/c nude mice were established [6] by inoculating SMMC-7721 cells (1×10^6 per mouse) in 50 μL of PBS containing BD Matrigel into right hind flank of 5-week-old mice or into the right upper liver lobe of 6-week-old mice, respectively. The orthotopic liver tumor was used for therapeutics studies 12 days after inoculation. Mice with a subcutaneous tumor size of 200–300 mm^3 were used for studies of biodistribution and imaging. Animals were handled under protocols approved by Soochow University Laboratory Animal Center, and the Animal Care and Use Committee of Soochow University.

2.6. In vivo pharmacokinetics and biodistribution of Tf-Ps-Dox

Tumor-free BALB/c mice were injected with 200 μL of Tf-Ps-Dox, Ps-Dox, or clinically used liposomal formulation (Lipo-Dox) at DOX dose of 4 mg/kg through tail veins (n = 3). At predetermined time points, approximately 20 μL of blood was withdrawn from the retro-orbital sinus of mice into heparinized tubes and immediately centrifuged. The plasma was taken and incubated overnight with 500 μL of DMF containing 20 mM DTT at 25 °C. After centrifugation, Dox in the supernatant was quantified using a fluorometer (Cary Eclipse, ex. 488 nm, em. 560 nm) and plotted as a function of time. The elimination half-lives and the area under the curve were derived.

In vivo targetability of Tf-Ps to subcutaneous SMMC 7721 tumor was investigated using near-infrared fluorescence imaging technique. Cy5-labeled polymer was incorporated to form Tf-Ps-Cy5 and Ps-Cy5, respectively. Briefly, 200 μL of Tf-Ps-Cy5 or Ps-Cy5 was *i.v.* injected into mice-bearing subcutaneous SMMC-7721 tumor (1.5 μg Cy5 equiv./mouse, n = 3). The fluorescence images were acquired at varied time intervals.

2.7. Anticancer therapy of Tf-Ps-Dox in mice bearing orthotopic SMMC-7721 tumor

The mice bearing orthotopic tumor were randomly grouped (n = 6), and 200 μL of Tf-Ps-Dox was injected through tail veins every four days (Dox dose: 8, 12, or 16 mg/kg, total 8 injections). Controls included PBS, Lipo-Dox (4 mg/kg), and Ps-Dox (8 mg/kg). Body weights of the mice were measured every two days and normalized to their initial weights. One mouse in each group was sacrificed on day 44, and heart, liver, spleen, lung, and kidney were taken for imaging and histological analyses (H&E staining and TUNEL staining). The survival rates, behavior changes, and liver ascites of the rest mice (n = 5) were monitored with time. Mice were also considered dead when the abdominal circumferences reached 100 mm due to liver ascites.

2.8. Statistical analysis

Difference between groups was determined using one-way ANOVA with Tukey multiple comparisons tests using Prism 7. Kaplan–Meier survival curves were constructed by log-rank test for comparisons using Prism 7. $^{*}p < 0.05$ was considered significant, and $^{**}p < 0.01$ and $^{***}p < 0.001$ were highly significant.

3. Results and discussion

3.1. Formation of Tf-Ps-Dox

Transferrin-guided polymersomal doxorubicin (Tf-Ps-Dox) was obtained by postmodification of maleimide-functionalized polymersomal doxorubicin (Mal-Ps-Dox) with thiolated transferrin (Tf-SH) (Scheme 1A). PEG-P(TMC-DTC) was selected in this study mainly owing to its unique features including biocompatibility, robust capacity of forming polymersome and Dox loading, reduction triggered drug release, decent stability, and facile surface functionalization for cellular targeting. Tf-SH was acquired with ca. 4 thiol groups per molecule, as shown by Ellman's assays, through treating Tf with Traut's Reagent under oxygen-free conditions at 37 °C for 1 h. Mal-Ps-Dox was fabricated with varying Mal molar surface densities from 3% to 10% and fixed Dox theoretical loading content of 16.7 wt%, from mPEG-P(TMC-DTC) and Mal-PEG-P (TMC-DTC), as reported previously for peptide-functionalized polymersomal doxorubicin [42,44]. The results showed that at a Tf-SH/Mal molar ratio of 2/1, rather consistent Tf conjugation efficiencies (70%–78%) as those of Mal-Ps-Dox, determined by BCA assays, were obtained (Table 1). Tf-Ps-Dox with Tf densities of 2.2%, 3.9%, 6.0%, and 7.0% were fabricated from Mal-Ps-Dox with Mal densities of 3%, 5%, 7%, and 10%, respectively. Notably, all four Tf-Ps-Dox exhibited a similar Dox loading content (10.1–10.6 wt%), small size (73–75 nm), and low polydispersity. Fig. 1A presents a typical size distribution profile of Tf-Ps-Dox. As expected, Tf-Ps-Dox was stable against extensive dilution or 10% serum (Fig. S1), owing to automatic disulfide-crosslinking of the membrane during fabrication [45–47]. The release mechanism of Dox from the polymersomes could be ascribed to the enhanced permeation of polymersomal membrane resulting from the de-crosslinking of polymersomes as triggered by the intracellular reduction environment (2–10 mM GSH).

Table 1
Characterization of Tf-Ps-Dox with varying Tf surface densities (Theoretical Dox loading content = 16.7 wt%).

Entry	Mal molar ratio (%)	Tf surface density (%)[a]	Conjugation efficiency (%)	Size (nm)[b]	PDI[b]	DLC[c] (wt.%)	DLE[c] (%)
1	3	2.2	73	73 ± 1	0.15	10.1	56
2	5	3.9	78	75 ± 2	0.16	10.6	59
3	8	6.0	75	75 ± 2	0.16	10.4	58
4	10	7.0	70	74 ± 2	0.17	10.5	58

[a] Determined by BCA assay.
[b] Determined by DLS.
[c] Determined by UV spectroscopy.

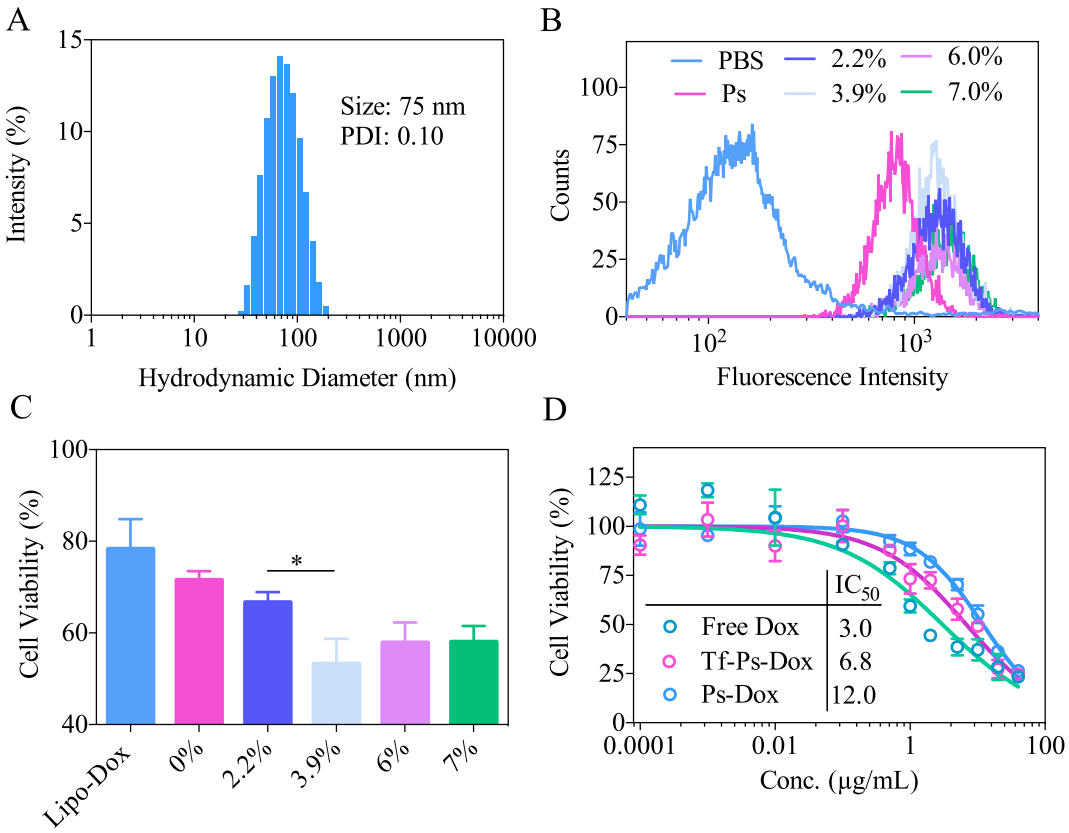

Fig. 1. *In vitro* characterization of Tf-Ps-Dox. (A) Hydrodynamic size distribution. (B) Flow cytometry of SMMC-7721 cells after 2 h of cultivation with Tf-Ps-Dox with varying Tf surface densities. Dox-loaded Ps and PBS were used as controls. (C) Viability of SMMC-7721 cells after 2 h of incubation with Tf-Ps-Dox or Lipo-Dox (5 μg Dox/mL) and 70 h of culture in fresh medium. (D) MTT assays of Tf-Ps-Dox to SMMC-7721 cells after 2 h of incubation and 70 h of culture in fresh medium.

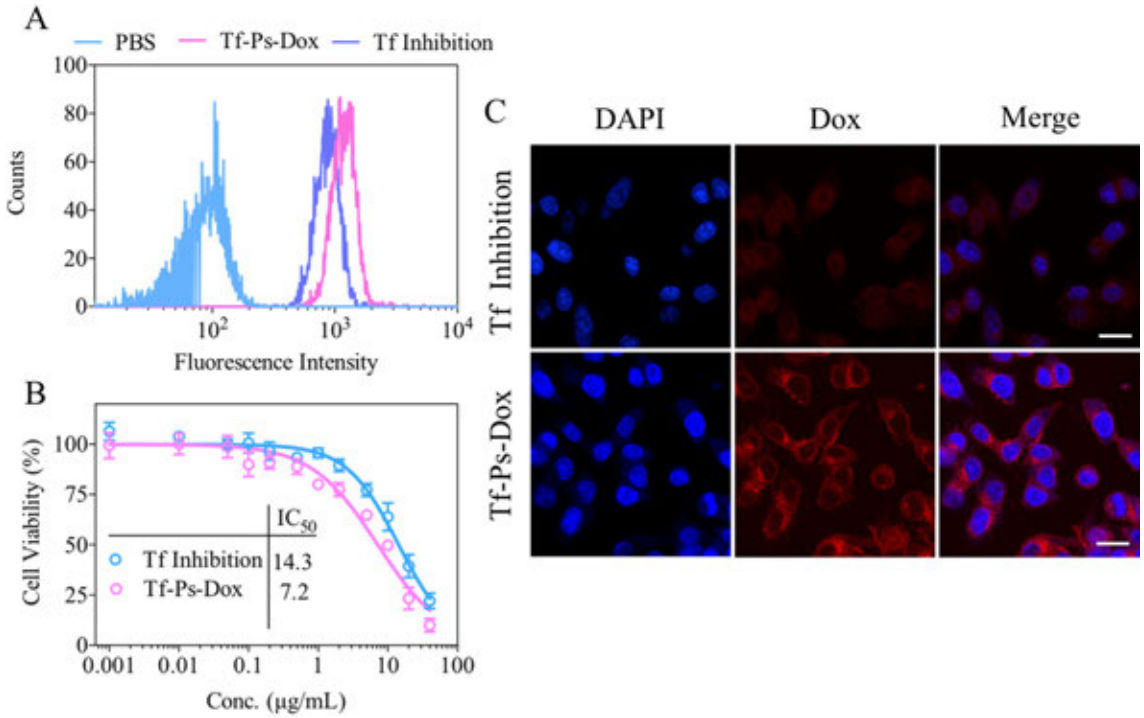

Fig. 2. The inhibition of cellular uptake and cell viability of SMMC-7721 cells treated by Tf-Ps-Dox for 2 h with or without adding 20 times excess free Tf, as measured by (A) flow cytometry, (B) MTT assays, and (C) CLSM images. Scale bar: 20 μm.

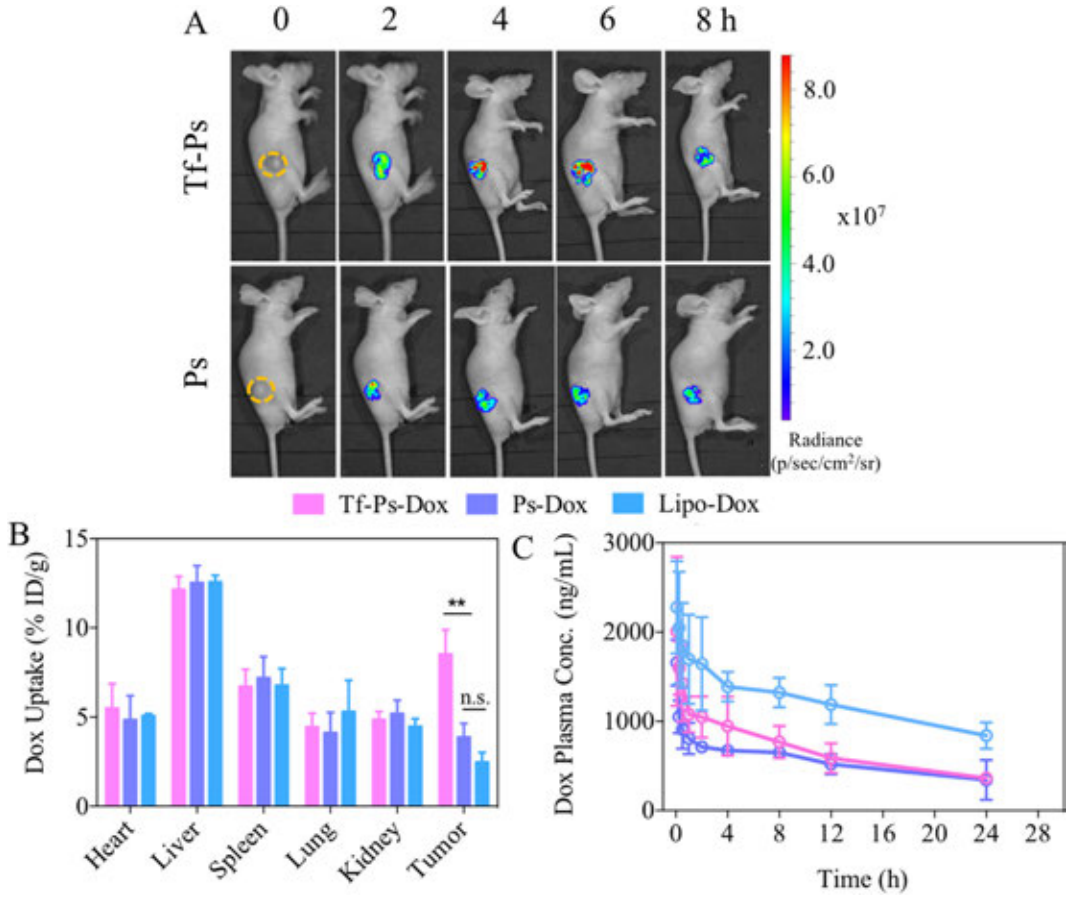

Fig. 3. *In vivo* imaging, biodistribution, and pharmacokinetics studies. (A) NIR images of mice bearing SMMC-7721 tumor at various time points after i.v. injection of Cy5-labeled Tf-Ps or Ps. (B) *In vivo* biodistribution of Dox in SMMC-7721 tumor-bearing mice treated by Tf-Ps-Dox (Dox dose: 10 mg/kg) at 6 h post injection. (C) Pharmacokinetics of Tf-Ps-Dox in BALB/c mice (Dox dose: 4 mg/kg). One-way ANOVA and Tukey multiple comparison tests, $^{**}p < 0.01$.

3.2. Specific antitumor effect of Tf-Ps-Dox toward SMMC-7721 cells

SMMC-7721 cells overexpressing transferrin receptor (TfR) [22] were employed to study the targetability of Tf-Ps-Dox. Flow cytometry showed that all four Tf-Ps-Dox formulations afforded approximately 2-fold higher cellular uptake than Ps-Dox (Fig. 1B), signifying that Tf-Ps-Dox could target to SMMC-7721 cells and Tf surface density is not critical for cell entry. Interestingly, MTT assays revealed that the antitumor activity of Tf-Ps-Dox is, however, highly dependent on Tf density, in which Tf-Ps-Dox with a Tf density of 3.9% produced the highest inhibitory effect to the cells (Fig. 1C). This is possibly due to the saturation of membrane TfR and/or too high avidity of Tf-Ps-Dox at high ligand densities to TfR. Davis et al. reported that a minimum Tf density was needed for efficient targeting *in vivo* [31], while too high or too low avidity of Tf to membrane TfR could lead to reduced tumor accumulation [48]. These results also indicate that Tf density has a great influence on the intracellular trafficking and/or drug release of Tf-Ps-Dox. We hereafter in later investigations selected Tf-Ps-Dox at a Tf density of 3.9% and referred it to Tf-Ps-Dox if not otherwise specified. Tf-Ps-Dox displayed a half-maximal inhibitory concentration (IC_{50}) toward SMMC-7721 cells of approximately 6.8 μg Dox equiv./mL, which, although higher than free Dox, was 2 times lower than that of Ps-Dox (Fig. 1D). Free Dox is known to be highly toxic to cells. The high systemic toxicity largely limits its direct application *in vivo*.

To verify that Tf-Ps-Dox was taken up by SMMC-7721 cells through TfR-mediated endocytosis, we performed competitive inhibition studies by co-incubating cells with 20-fold excess free Tf. Flow cytometry showed clearly that uptake of Tf-Ps-Dox by SMMC-7721 cells was reduced to half when co-incubated with free Tf (Fig. 2A), proving a TfR-mediated uptake mechanism for Tf-Ps-Dox. Accordingly, the IC_{50} of Tf-Ps-Dox was also truncated to half by co-incubation with 20-fold excess of free Tf (Fig. 2B), becoming similar to that of the non-targeted Ps-Dox. CLSM images showed that Tf-Ps-Dox-treated cells had much more intense Dox fluorescence than the free Tf co-cultured group (Fig. 2C). All the above results support that Tf-Ps-Dox actively targets to SMMC-7721 hepatocellular carcinoma cells through TfR.

3.3. In vivo biodistribution and pharmacokinetics

The *in vivo* fluorescence images of subcutaneous SMMC-7721 tumors monitored over time following *i.v.* injection of Cy5-labeled blank Tf-Ps showed fast and obviously better tumor accumulation than Cy5-labeled blank Ps (nontargeted control), in which maximum Cy5 fluorescence in tumor was discerned at 6 h postinjection (Fig. 3A). Then Dox contents in the tumors and major organs of mice treated by Tf-Ps-Dox at 6 h post-injection were quantified, and the tumor accumulation of 8.5% ID/g was achieved, which was, respectively, ca. 2 or 3 times that of Ps-Dox or Lipo-Dox, respectively (Fig. 3B). This targeted tumor accumulation of

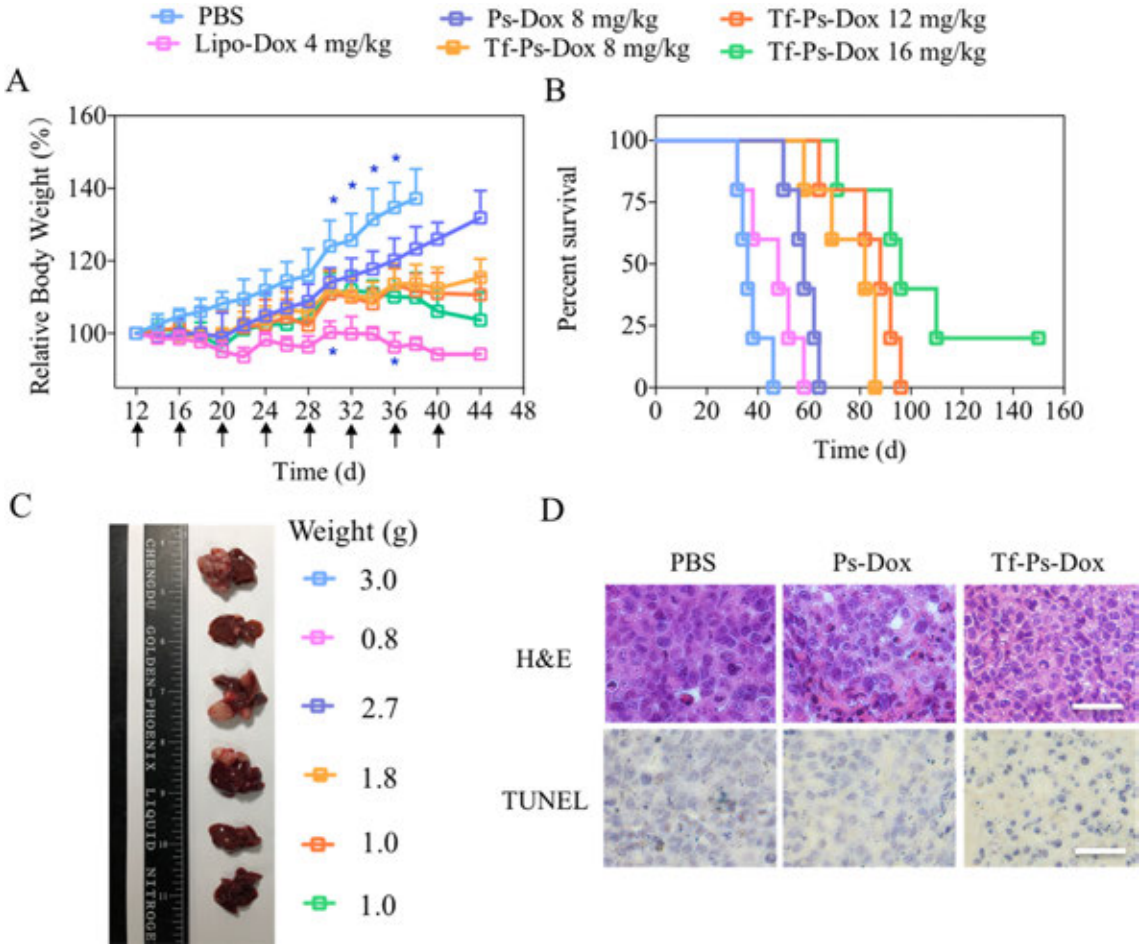

Fig. 4. *In vivo* antitumor activity of Tf-Ps-Dox in orthotopic SMMC-7721 tumor-bearing mice (n = 6) with drug administration every 4 days (total 8 injections). (A) Relative body weight changes. (B) Survival curves. Statistical analysis (Kaplan–Meier analysis, log-rank test): Ps-Dox (8 mg/kg) *vs.* PBS: $^{**}p < 0.01$; Lipo-Dox (4 mg/kg) *vs.* PBS: n.s.; Ps-Dox (8 mg/kg) *vs.* Lipo-Dox (4 mg/kg): n.s.; Tf-Ps-Dox (8 mg/kg) *vs.* Lipo-Dox (4 mg/kg) and Ps-Dox (8 mg/kg): $^{**}p < 0.01$; Tf-Ps-Dox (16 mg/kg) *vs.* Tf-Ps-Dox (8 mg/kg): $^{*}p < 0.05$. (C) The photograph of livers excised on 44 days. (D) Images of H&E and TUNEL stained tumor slices from mice treated with PBS, Ps-Dox (8 mg/kg), or Tf-Ps-Dox (8 mg/kg). Scale bar: 50 μm.

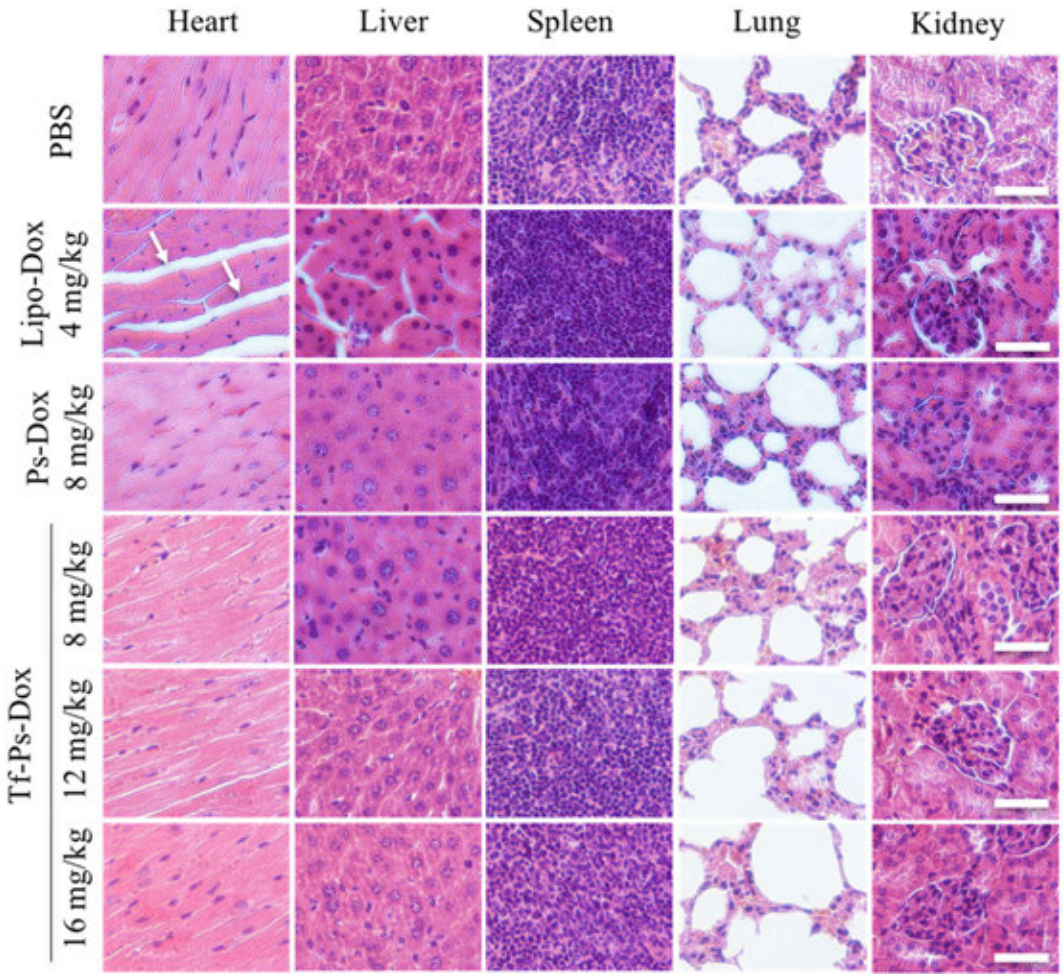

Fig. 5. H&E-stained heart, liver, spleen, lung, and kidney sections excised from mice after different treatments (400×). Scale bar: 50 μm.

the drug was higher than that of Dox-loaded folic acid-modified nanoparticles (5% ID/g) [49]. The similar enhanced tumor uptake (ca. 3-fold) was found for PTX-loaded glycyrrhizin-directed nanoparticles [50]. In contrast, no significant difference in the Dox level was detected in the major organs for Tf-Ps-Dox and Ps-Dox. Hence, these results indicate that Tf can specifically improve the HCC accumulation of Ps-Dox.

We further investigated the pharmacokinetics of Tf-Ps-Dox in BALB/c mice. It was showed that Tf-Ps-Dox could circulate for a long time in mice and had an elimination half-life was 8.7 h, which was comparable to that of nontargeted Ps-Dox (8.2 h) but shorter than Lipo-Dox (16.9 h, Fig. 3C). The results prove that Tf-Ps-Dox indeed has remarkable *in vivo* stability and that the Tf-functionalization does not shorten their blood circulation.

3.4. Therapy of mice with orthotopic SMMC-7721 tumor

These tumor-bearing mice that received only PBS developed severe liver ascites starting from 26 days post tumor inoculation and abnormal increase in body weights (Fig. 4A). The mice became apathetic and weak with time. These results indicate successful establishment of orthotopic SMMC-7721 tumor in the liver. During the treatment, the mice were judged dead if body weight loss was more than 15% as compared to the original weight or if the abdominal circumference exceeded 100 mm. All PBS-treated mice died within 42 days (Fig. 4B). In sharp contrast, the mice that received Tf-Ps-Dox treatment at varying doses from 8, 12, to 16 mg/kg every 4 days (8 injections in total) were mostly without liver ascites in 40 days, in which the increase in body weights was largely inhibited (Fig. 4A). The nontargeted Ps-Dox group revealed, although some antitumor effect, apparently more liver ascites and body weight increase than the Tf-Ps-Dox group. Considering the injection frequency and the total dose of Dox, Lipo-Dox at 8 mg/kg was not studied for comparison owing to serious side effects [51]. Lipo-Dox (4 mg/kg) was selected as control instead. However, it also caused systematic toxicity over repeated intravenous injection, including significant body weight loss (Fig. 4A) and pronounced hand-food syndrome (HFS) of the mice. Similarly, Webster et al. reported that galactosylated chitosan triptolide nanoparticle-treated mice with orthotopic HCC only revealed slight body weight change, in contrast to an apparent weight loss of the nontargeted group resulting from severe side effects and significant body weight increase in the PBS group [52]. As shown in the survival curves, Lipo-Dox treatment to the mice did not improve the survival rate as compared to the PBS group (Fig. 4B). The survival rate was, however, significantly improved by treating with Ps-Dox or Tf-Ps-Dox at 8 mg/kg, in which the median survival times were 58 and 82 days, respectively. In addition, the median survival times could be further increased to 88 and 96 days by increasing the dose of Tf-Ps-Dox to 12 and 16 mg/kg, respectively. Of note, 1 out of 5 mice receiving Tf-Ps-Dox (16 mg/kg) revealed complete regression (CR). This median survival time was much longer than that of 5-fluorouracil nanoparticle-treated mice with orthotopic SMMC-7721 tumor (35 days) [53].

Fig. 4C shows the *ex-vivo* photographs of livers excised from different treatment groups on day 44. At 8 mg/kg, Tf-Ps-Dox induced apparently better tumor suppression than Ps-Dox. Notably, the mice treated with Tf-Ps-Dox at 12 and 16 mg/kg bare significantly fewer tumor spots in the livers. The histological assays of H&E or TUNEL stained slices of orthotopic liver tumors displayed distinct differences between PBS, Ps-Dox, and Tf-Ps-Dox groups. From TUNEL assays, the Tf-Ps-Dox group showed significant decrease of tumor burden and increase of tumor apoptosis compared with the PBS group (Fig. 4D). While in H&E-stained tumor slices, Tf-Ps-Dox-treated tumors displayed much more nuclear-lysis, incomplete cell membrane, and cell shrinkage than the Ps-Dox group, in contrast to the PBS group. In addition, H&E-stained slices of the major organs exhibited that Tf-Ps-Dox instigated no obvious side effects to normal organs (Figs. 5, S2). However, Lipo-Dox caused damage not only to the liver but also to the heart tissue. For instance, after repeated injection of Lipo-Dox, the liver tissue structure became incomplete, the liver plate was not arranged neatly, and some hepatocyte nuclear vacuolar degeneration occurred (Fig. S3). In addition, abnormal shape and arrangement was found in cardiomyocytes.

4. Conclusion

We have established that transferrin-guided polymersomal doxorubicin (Tf-Ps-Dox) can be easily fabricated with controlled transferrin density, small size, and high drug loading through ligand postmodification strategy. Functionalization of Ps-Dox with 3.9% Tf caused better uptake and specific antitumor effect toward transferrin receptor overexpressed human SMMC-7721 cells. *In vivo* experiments revealed that Tf-Ps-Dox can actively target to orthotopic SMMC-7721 tumor in mice, leading to 2–3 times better tumor accumulation and significantly improved survival time than non-targeted Ps-Dox and clinically viable liposomal Dox formulation (Lipo-Dox). Particularly, Tf-Ps-Dox at doses of 8 to 16 mg/kg resulted in visibly lesser systemic toxicity than Lipo-Dox at 4 mg/kg. Transferrin-guided polymersomal doxorubicin has appeared to be appealing for targeted hepatocellular carcinoma chemotherapy.

Acknowledgment

This work is supported by research grants from the National Natural Science Foundation of China (NSFC 51761135117, 51633005, 51561135010, 51861145310, 51773146, and 51473111).

Appendix A. Supplementary data

Supplementary data to this article can be found online at https://doi.org/10.1016/j.actbio.2019.05.034.

References

[1] B. Njei, Y. Rotman, I. Ditah, J.K. Lim, Emerging trends in hepatocellular carcinoma incidence and mortality, Hepatology 61 (2015) 191–199.
[2] A. Fomer, M. Gilabert, J. Bruix, J.L. Raoul, Treatment of intermediate-stage hepatocellular carcinoma, Nat. Rev. Clin. Oncol. 11 (2014) 525–535.
[3] N.K. Mohamed, M.A. Hamad, M.Z.E. Hafez, K.L. Wooley, M. Elsabahy, Nanomedicine in management of hepatocellular carcinoma: challenges and opportunities, Int. J. Cancer 140 (2017) 1475–1484.
[4] A. Lamprecht, Nanomedicines in gastroenterology and hepatology, Nat. Rev. Gastroenterol. Hepatol. 12 (2015) 195–204.
[5] Y.D. Livney, Y.G. Assaraf, Rationally designed nanovehicles to overcome cancer chemoresistance, Adv. Drug Delivery Rev. 65 (2013) 1716–1730.
[6] Y. Fang, W.J. Yang, L. Cheng, F.H. Meng, J. Zhang, Z.Y. Zhong, EGFR-targeted multifunctional polymersomal doxorubicin induces selective and potent suppression of orthotopic human liver cancer in vivo, Acta Biomater. 64 (2017) 323–333.
[7] D.Y. Gao, T.T. Lin, Y.C. Sung, Y.C. Liu, W.H. Chiang, C.C. Chang, J.Y. Liu, Y.C. Chen, CXCR4-targeted lipid-coated PLGA nanoparticles deliver sorafenib and overcome acquired drug resistance in liver cancer, Biomaterials 67 (2015) 194–203.
[8] J. Gao, H.W. Chen, Y.S. Yu, J.J. Song, H. Song, X. Su, W. Li, X. Tong, W.Z. Qian, H. Wang, J.X. Dai, Y.J. Guo, Inhibition of hepatocellular carcinoma growth using immunoliposomes for co-delivery of adriamycin and ribonucleotide reductase M2 siRNA, Biomaterials 34 (2013) 10084–10098.
[9] J. Gao, Y.S. Yu, Y.Y. Zhang, J.J. Song, H.W. Chen, W. Li, W.Z. Qian, L. Deng, G. Kou, J.M. Chen, Y.J. Guo, EGFR-specific PEGylated immunoliposomes for active siRNA delivery in hepatocellular carcinoma, Biomaterials 33 (2012) 270–282.
[10] T.P. Guan, W.T. Shang, H. Li, X. Yang, C.H. Fang, J. Tian, K. Wang, From detection to resection: photoacoustic tomography and surgery guidance with indocyanine green loaded gold Nanorod@liposome core-shell nanoparticles in liver cancer, Bioconjug. Chem. 28 (2017) 1221–1228.
[11] Y.K. Kim, A. Minai-Tehrani, J.H. Lee, C.S. Cho, M.H. Cho, H.L. Jiang, Therapeutic efficiency of folated poly(ethylene glycol)-chitosan-graft-polyethylenimine-Pdcd4 complexes in H-ras12V mice with liver cancer, Int. J. Nanomed. 8 (2013) 1489–1498.
[12] X.B. Ma, H. Hui, Y.S. Jin, D. Dong, X.L. Liang, X. Yang, K. Tan, Z.F. Dai, Z. Cheng, J. Tian, Enhanced immunotherapy of SM5-1 in hepatocellular carcinoma by conjugating with gold nanoparticles and its in vivo bioluminescence tomographic evaluation, Biomaterials 87 (2016) 46–56.
[13] D. Shao, J. Li, X. Zheng, Y. Pan, Z. Wang, M. Zhang, Q.X. Chen, W.F. Dong, L. Chen, Janus "nano-bullets" for magnetic targeting liver cancer chemotherapy, Biomaterials 100 (2016) 118–133.
[14] B. Singh, Y. Jang, S. Maharjan, H.J. Kim, A.Y. Lee, S. Kim, N. Gankhuyag, M.S. Yang, Y.J. Choi, M.H. Cho, C.S. Cho, Combination therapy with doxorubicin-loaded galactosylated poly(ethyleneglycol)-lithocholic acid to suppress the tumor growth in an orthotopic mouse model of liver cancer, Biomaterials 116 (2017) 130–144.
[15] L.F. Tan, S.P. Wang, K. Xu, T.L. Liu, P. Liang, M. Niu, C.H. Fu, H.B. Shao, J. Yu, T.C. Ma, X.L. Ren, H. Li, J.P. Dou, J. Ren, X.W. Meng, Layered MoS2 hollow spheres for highly-efficient photothermal therapy of rabbit liver orthotopic transplantation tumors, Small 12 (2016) 2046–2055.
[16] J. Wang, Z.H. Zhang, X. Wang, W. Wu, X.Q. Jiang, Size- and pathotropism-driven targeting and washout-resistant effects of boronic acid-rich protein nanoparticles for liver cancer regression, J. Control. Release 168 (2013) 1–9.
[17] H.J. Zhang, N. Patel, S. Ding, J. Xiong, P.P. Wu, Theranostics for hepatocellular carcinoma with Fe3O4@ZnO nanocomposites, Biomater. Sci. 4 (2016) 288–298.
[18] X.X. Zhang, S.Y. Guo, R. Fan, M.R. Yu, F.F. Li, C.L. Zhu, Y. Gan, Dual-functional liposome for tumor targeting and overcoming multidrug resistance in hepatocellular carcinoma cells, Biomaterials 33 (2012) 7103–7114.
[19] L.N. Wang, W.J. Su, Z. Liu, M.Q. Zhou, S. Chen, Y.A. Chen, D. Lu, Y.H. Liu, Y. Fan, Y.Z. Zheng, Z.C. Han, D.L. Kong, J.C. Wu, R. Xiang, Z.J. Li, CD44 antibody-targeted liposomal nanoparticles for molecular imaging and therapy of hepatocellular carcinoma, Biomaterials 33 (2012) 5107–5114.
[20] H.P. Xia, F.Y. Li, W. Park, S.F. Wang, Y. Jang, Y. Du, S. Baik, S. Cho, T. Kang, D.H. Kim, D.S. Ling, K.M. Hui, T. Hyeon, pH-sensitive Pt nanocluster assembly overcomes cisplatin resistance and heterogeneous stemness of hepatocellular carcinoma, ACS Central Sci. 2 (2016) 802–811.
[21] J.L. Lv, H.L. Sun, Y. Zou, F.H. Meng, A.A. Dias, M. Hendriks, J. Feijen, Z.Y. Zhong, Reductively degradable alpha-amino acid-based poly(ester amide)-graft-galactose copolymers: facile synthesis, self-assembly, and hepatoma-targeting doxorubicin delivery, Biomater. Sci. 3 (2015) 1134–1146.
[22] K.L. Fan, C.Q. Cao, Y.X. Pan, D. Lu, D.L. Yang, J. Feng, L.N. Song, M.M. Liang, X.Y. Yan, Magnetoferritin nanoparticles for targeting and visualizing tumour tissues, Nat. Nanotechnol. 7 (2012) 459–464.
[23] M.S. Muthu, R.V. Kutty, Z.T. Luo, J.P. Xie, S.S. Feng, Theranostic vitamin E TPGS micelles of transferrin conjugation for targeted co-delivery of docetaxel and ultra bright gold nanoclusters, Biomaterials 39 (2015) 234–248.
[24] T. Kang, M.Y. Jiang, D. Jiang, X.Y. Feng, J.H. Yao, Q.X. Song, H.Z. Chen, X.L. Gao, J. Chen, Enhancing glioblastoma-specific penetration by functionalization of nanoparticles with an iron-mimic peptide targeting transferrin/transferrin receptor complex, Mol. Pharm. 12 (2015) 2947–2961.
[25] H. Makwana, F. Mastrotto, J.P. Magnusson, D. Sleep, J. Hay, K.J. Nicholls, S. Allen, C. Alexander, Engineered polymer-transferrin conjugates as self-assembling targeted drug delivery systems, Biomacromolecules 18 (2017) 1532–1543.
[26] K.B. Johnsen, T. Moos, Revisiting nanoparticle technology for blood-brain barrier transport: unfolding at the endothelial gate improves the fate of transferrin receptor-targeted liposomes, J. Control. Release 222 (2016) 32–46.
[27] S. Tortorella, T.C. Karagiannis, Transferrin receptor-mediated endocytosis: a useful target for cancer therapy, J. Membr. Biol. 247 (2014) 291–307.
[28] T.C. Karagiannis, P.N. Lobachevsky, B.K.Y. Leung, J.M. White, R.F. Martin, Receptor-mediated DNA-targeted photoimmunotherapy, Cancer Res. 66 (2006) 10548–10552.
[29] M. Szwed, A. Matusiak, A. Laroche-Clary, J. Robert, I. Marszalek, Z. Jozwiak, Transferrin as a drug carrier: cytotoxicity, cellular uptake and transport kinetics of doxorubicin transferrin conjugate in the human leukemia cells, Toxicol. In Vitro 28 (2014) 187–197.
[30] S. Bae, K. Ma, T.H. Kim, E.S. Lee, K.T. Oh, E.S. Park, K.C. Lee, Y.S. Youn, Doxorubicin-loaded human serum albumin nanoparticles surface-modified with TNF-related apoptosis-inducing ligand and transferrin for targeting multiple tumor types, Biomaterials 33 (2012) 1536–1546.

[31] C.H.J. Choi, C.A. Alabi, P. Webster, M.E. Davis, Mechanism of active targeting in solid tumors with transferrin-containing gold nanoparticles, Proc. Natl. Acad. Sci. U. S. A. 107 (2010) 1235–1240.
[32] A.J. Clark, M.E. Davis, Increased brain uptake of targeted nanoparticles by adding an acid-cleavable linkage between transferrin and the nanoparticle core, Proc. Natl. Acad. Sci. U. S. A. 112 (2015) 12486–12491.
[33] Y.N. Cui, Q.X. Xu, P.K.H. Chow, D.P. Wang, C.H. Wang, Transferrin-conjugated magnetic silica PLGA nanoparticles loaded with doxorubicin and paclitaxel for brain glioma treatment, Biomaterials 34 (2013) 8511–8520.
[34] J. Wang, S.M. Tian, R.A. Petros, M.E. Napier, J.M. DeSimone, The complex role of multivalency in nanoparticles targeting the transferrin receptor for cancer therapies, J. Am. Chem. Soc. 132 (2010) 11306–11313.
[35] Z.G. Yang, B. Yu, J. Zhu, X.M. Huang, J. Xie, S.L. Xu, X.J. Yang, X.M. Wang, B.C. Yung, L.J. Lee, R.J. Lee, L.S. Teng, A microfluidic method to synthesize transferrin-lipid nanoparticles loaded with siRNA LOR-1284 for therapy of acute myeloid leukemia, Nanoscale 6 (2014) 9742–9751.
[36] H.J. Zhang, L. Hou, X.J. Jiao, Y.D. Ji, X.L. Zhu, Z.Z. Zhang, Transferrin-mediated fullerenes nanoparticles as Fe2+-dependent drug vehicles for synergistic anti-tumor efficacy, Biomaterials 37 (2015) 353–366.
[37] F.C. Lam, S.W. Morton, J. Wyckoff, T.L.V. Han, M.K. Hwang, A. Maffa, E. Balkanska-Sinclair, M.B. Yaffe, S.R. Floyd, P.T. Hammond, Enhanced efficacy of combined temozolomide and bromodomain inhibitor therapy for gliomas using targeted nanoparticles, Nat. Commun. 9 (2018) 11.
[38] R. van der Meel, L.J.C. Vehmeijer, R.J. Kok, G. Storm, E.V.B. van Gaal, Ligand-targeted particulate nanomedicines undergoing clinical evaluation: current status, Adv. Drug Delivery Rev. 65 (2013) 1284–1298.
[39] R. Suzuki, T. Takizawa, Y. Kuwata, M. Mutoh, N. Ishiguro, N. Utoguchi, A. Shinohara, M. Eriguchi, H. Yanagie, K. Maruyama, Effective anti-tumor activity of oxaliplatin encapsulated in transferrin-PEG-liposome, Int. J. Pharm. 346 (2008) 143–150.
[40] M.E. Davis, J.E. Zuckerman, C.H.J. Choi, D. Seligson, A. Tolcher, C.A. Alabi, Y. Yen, J.D. Heidel, A. Ribas, Evidence of RNAi in humans from systemically administered siRNA via targeted nanoparticles, Nature 464 (2010) 1067–1070.
[41] N.C. Bellocq, S.H. Pun, G.S. Jensen, M.E. Davis, Transferrin-containing, cyclodextrin polymer-based particles for tumor-targeted gene delivery, Bioconjug. Chem. 14 (2003) 1122–1132.
[42] Y. Zou, F.H. Meng, C. Deng, Z.Y. Zhong, Robust, tumor-homing and redox-sensitive polymersomal doxorubicin: a superior alternative to Doxil and Caelyx?, J Control. Release 239 (2016) 149–158.
[43] G.L. Ellman, A colorimetric method for determining low concentrations of mercaptans, Arch. Biochem. Biophys. 74 (1958) 443–450.
[44] N. Zhang, Y.F. Xia, Y. Zou, W.J. Yang, J. Zhang, Z.Y. Zhong, F.H. Meng, ATN-161 peptide functionalized reversibly cross-linked polymersomes mediate targeted doxorubicin delivery into melanoma-bearing C57BL/6 mice, Mol. Pharm. 14 (2017) 2538–2547.
[45] W.J. Yang, Y. Zou, F.H. Meng, J. Zhang, R. Cheng, C. Deng, Z.Y. Zhong, Efficient and targeted suppression of human lung tumor xenografts in mice with methotrexate sodium encapsulated in all-function-in-one chimeric polymersomes, Adv. Mater. 28 (2016) 8234–8239.
[46] Y. Jiang, J. Zhang, F. Meng, Z. Zhong, Apolipoprotein E peptide-directed chimeric polymersomes mediate an ultrahigh-efficiency targeted protein therapy for glioblastoma, ACS Nano 12 (2018) 11070–11079.
[47] W.J. Yang, Y.H. Wei, L. Yang, J. Zhang, Z.Y. Zhong, G. Storm, F.H. Meng, Granzyme B-loaded, cell-selective penetrating and reduction-responsive polymersomes effectively inhibit progression of orthotopic human lung tumor in vivo, J. Control. Release 290 (2018) 141–149.
[48] D.T. Wiley, P. Webster, A. Gale, M.E. Davis, Transcytosis and brain uptake of transferrin-containing nanoparticles by tuning avidity to transferrin receptor, Proc. Natl. Acad. Sci. U. S. A. 110 (2013) 8662–8667.
[49] J.J. Wu, C. Tang, C.H. Yin, Co-delivery of doxorubicin and interleukin-2 via chitosan based nanoparticles for enhanced antitumor efficacy, Acta Biomater. 47 (2017) 81–90.
[50] L.L. Shi, C. Tang, C.H. Yin, Glycyrrhizin-modified O-carboxymethyl chitosan nanoparticles as drug vehicles targeting hepatocellular carcinoma, Biomaterials 33 (2012) 7594–7604.
[51] Y. Zou, Y.F. Xia, F.H. Meng, J. Zhang, Z.Y. Zhong, GE11-directed functional polymersomal doxorubicin as an advanced alternative to clinical liposomal formulation for ovarian cancer treatment, Mol. Pharm. 15 (2018) 3664–3671.
[52] Y.Q. Zhang, Y. Shen, M.M. Liao, X. Mao, G.J. Mi, C. You, Q.Y. Guo, W.J. Li, X.Y. Wang, N. Lin, T.J. Webster, Galactosylated chitosan triptolide nanoparticles for overcoming hepatocellular carcinoma: enhanced therapeutic efficacy, low toxicity, and validated network regulatory mechanisms, Nanomed.-Nanotechnol. Biol. Med. 15 (2019) 86–97.
[53] M.R. Cheng, B. He, T. Wan, W.P. Zhu, J. Han, B.B. Zha, H.X. Chen, F.X. Yang, Q. Li, W. Wang, H.Z. Xu, T. Ye, 5-Fluorouracil nanoparticles inhibit hepatocellular carcinoma via activation of the p53 pathway in the orthotopic transplant mouse model, PLoS ONE 7 (2012) e47115.